WIDE-ANGLE SAR IMAGE FORMATION WITH MIGRATORY SCATTERING CENTERS AND REGULARIZATION IN HOUGH SPACE

Kush R. Varshney, Müjdat Çetin, John W. Fisher III, and Alan S. Willsky

Massachusetts Institute of Technology
77 Massachusetts Avenue
Cambridge, Massachusetts 02139
krv@mit.edu, mcetin@mit.edu, fisher@csail.mit.edu, willsky@mit.edu

ABSTRACT

Wide-angle synthetic aperture radar imaging presents numerous challenges, but also opportunities to extract object-level information. We present a methodology using an overcomplete dictionary and sparsifying regularization to characterize anisotropy (aspect-dependent scattering amplitude), and migration (aspect-dependent scattering center spatial location), into the image formation process. We also introduce regularization terms in the normal parameter space of the Hough transform that favor solutions with sparsity along a line and consequently parsimony in the representation of glint anisotropy. The characterization of scatterer migration directly gives information about size and shape of objects in the spatial domain and such information can also be inferred from the parsimonious representations we extract for glint-type scattering.

1. INTRODUCTION

The ultimate goal in imaging is understanding what is out in the scene being observed. First steps towards this goal include the collection of measurements and the formation of imagery from those measurements. In synthetic aperture radar (SAR) imaging, data collected over wide-angle apertures permits, in principle, the reconstruction of images with high cross-range resolution. However, conventional SAR image formation techniques, such as the polar format algorithm [1], do not account for certain physical phenomena that arise in wide-angle imaging, leading to inaccurate scattering estimates. In addition, conventional techniques do not extract all possible information from SAR measurements that could be used in higher level scene understanding tasks. In this paper, we propose methods that mitigate these shortcomings of conventional image formation techniques.

In spotlight-mode SAR, measurements are acquired using a radar set mounted on an aircraft. As the aircraft proceeds along its flight path, the radar is continually steered so that it illuminates the same ground patch from all aspect angles of data collection. Recent advances in navigation and avionics technologies now allow long flight paths, or wide-angle apertures. However, dependence of scattering behavior on aspect angle, termed anisotropy, becomes an issue because objects are viewed from different sides rather than from nearly the same point of view. For example, a mirror or flat metal sheet may reflect strongly when viewed straight on, but barely reflect at all from an oblique angle. This is in opposition to narrow-angle imaging, where it is a fairly reasonable assumption that scattering amplitude is constant over the aperture. In addition, certain scattering mechanisms, such as tophats and cylinders, appear to migrate or move in their spatial location as a function of aspect angle with wide-angle apertures [2].

There are various approaches for anisotropy characterization including parametric methods [3, 4, 5] and methods based on subaperture analysis, in which the full collection of SAR measurements is divided into smaller segments covering only parts of the wide-angle aperture and a different image is formed for each subaperture [6, 7, 8]. In our previous work, we developed a method for joint image formation and anisotropy characterization based on an overcomplete dictionary and sparsifying regularization [9]. The characterization of migratory scattering has not been given much heed in previous work. In the first part of this paper, we extend our overcomplete dictionary for characterizing anisotropy to account for migratory scattering.

Non-migratory scattering exhibits an interesting relationship between anisotropy and physical extent in the spatial domain. Scattering response over only a very small range of aspect angles, known as glint or flash, arises from long, flat plates, and the thinner the anisotropic response, the longer the spatial extent of the plate. The aspect angle of the glint is also the orientation of the object in space. In the second part of the paper, utilizing Hough transform properties, we introduce new regularization terms to favor solutions that concentrate the representation of glint anisotropy across a spatially distributed area into a single scatterer.

2. SAR OBSERVATION MODEL WITH ANISOTROPIC AND MIGRATORY SCATTERING

The response to radar illumination by the ground patch being observed may be expressed as a complex-valued scattering function $s(x, y)$, where x and y are coordinates on the ground. It is this $s(x, y)$ that conventional image formation techniques attempt to recover. With anisotropy, the scattering function also depends on aspect angle θ, and is thus $s(x, y, \theta)$. At typical operating frequencies of SAR, it is a reasonable assumption that scattering comes from a discrete set of points rather than a continuous field [10]. Measurements are obtained in what is known as the phase history domain. Setting aside migratory scattering in this preliminary exposition, with P point-scatterers the measurements and scattering

This work was partially supported by the Air Force Research Laboratory under Grant FA8650-04-1-1719, and Grant FA8650-04-C-1703 (through subcontract 04079-6918 from BAE Systems Advanced Information Technologies). The first author is supported by a National Science Foundation Graduate Research Fellowship.

function are related by the following expression:

$$r\left(f,\theta\right)=\sum_{p=1}^{P}s\left(x_p,y_p,\theta\right)e^{-j\frac{4\pi f}{c}\left(x_p\cos\theta+y_p\sin\theta\right)}, \quad (1)$$

where c is the speed of propagation and f is frequency. Measurements are discrete, at N angles θ_n and K frequencies f_k.

Another domain in which SAR data may be viewed is the range profile domain. The phase history domain and range profile domain are related by a one-dimensional Fourier transform; ideally, the range profile expression is:

$$\hat{R}\left(\rho,\theta\right)=\sum_{p=1}^{P}s\left(x_p,y_p,\theta\right)\delta\left(\rho-x_p\cos\theta-y_p\sin\theta\right), \quad (2)$$

where ρ parameterizes distance along the line of sight of the radar at aspect angle θ, but because measurements are at a finite set of frequencies f_k within a certain frequency band, there are sidelobe effects. For a single point-scatterer, ideally the range profile is non-zero on a sinusoid $\rho(\theta)=x_0\cos\theta+y_0\sin\theta$.

Now, let us consider migratory scattering. Migration occurs when radar pulses bounce back from the closest surface of a physical object, but the closest surface of the object is different from different viewing angles; the physical object is not really moving, but appears to move in the measurement domain. For the moment restricting ourselves to migration around a circle with center (x_c,y_c) and radius R_0, which could be due to a cylinder or tophat, we note that the point on the circle at angle θ is $(x_c-R_0\cos\theta,y_c-R_0\sin\theta)$. Thus, the sinusoid expression changes to:

$$\begin{aligned}\rho(\theta)&=(x_c-R_0\cos\theta)\cos\theta+(y_c-R_0\sin\theta)\sin\theta\\&=x_c\cos\theta+y_c\sin\theta-R_0. \quad (3)\end{aligned}$$

Another way to come upon this expression is to consider the fact that at all aspect angles, the surface of the circle is closer to the radar by R_0 than the center. For any general convex shape of migration, the form $x_c\cos\theta+y_c\sin\theta-R(\theta)$ is taken.

In discussing stationary scattering centers, the spatial location (x_p,y_p) and the scattering center p are synonymous. However, care must be taken when discussing migratory scattering centers — some invariant location $(\bar{x}_p,\bar{y}_p)$ is needed to discuss the function $s(\bar{x}_p,\bar{y}_p,\theta)$ for example. We take this invariant spatial location $(\bar{x}_p,\bar{y}_p)$ to be the location the scattering center appears at when $\theta=0$. When $\theta=0$, $\bar{x}=x_c-R(0)$ and $\bar{y}=y_c$, leading to the following expression for phase history with migratory point scatterers:

$$r\left(f,\theta\right)=\sum_{p=1}^{P}s\left(\bar{x}_p,\bar{y}_p,\theta\right)e^{-j\frac{4\pi f}{c}\left(\left(\bar{x}_p+R_p(0)\right)\cos\theta+\bar{y}_p\sin\theta-R_p(\theta)\right)}. \quad (4)$$

3. OVERCOMPLETE DICTIONARY AND SPARSIFYING REGULARIZATION FORMULATION

The approach we followed in [9] for anisotropy characterization was to construct an overcomplete expansion of aspect-dependent scattering with $M>N$ atoms per spatial location. We extend that approach here by taking LM atoms per spatial location, where we do a further expansion in radius of migration with L different values for the radius. (We have once again restricted ourselves to the important case of migration in a circle.)

Specifically, we have PLM coefficients $a_{p,l,m}$ and the overcomplete expansion in the phase history domain is as follows:

$$r\left(f,\theta\right)=\sum_{p=1}^{P}\sum_{l=1}^{L}\sum_{m=1}^{M}a_{p,l,m}b_m\left(\theta\right)e^{-j\frac{4\pi f}{c}\left(\left(\bar{x}_p+R_l\right)\cos\theta+\bar{y}_p\sin\theta-R_l\right)}. \quad (5)$$

The $b_m(\theta)$ represent different persistence widths and center angles of contiguous intervals of anisotropy; more details may be found in [9]. Making the appropriate definitions, the expansion into the overcomplete dictionary can be expressed as:

$$r\left(f,\theta\right)=\sum_{p=1}^{P}\sum_{l=1}^{L}\sum_{m=1}^{M}a_{p,l,m}\phi_{p,l,m}\left(\theta\right). \quad (6)$$

Each atom $\phi_{p,l,m}(\theta)$ corresponds to a different invariant spatial location, different radius of migration, and different anisotropy. By appropriately stacking the phase history measurements into an $NK\times1$ vector $\mathbf{r}$, concatenating all of the atoms into an $NK\times LMP$ matrix $\mathbf{\Phi}$, and taking the coefficients as an $LMP\times1$ vector $\mathbf{a}$, we can also write the overcomplete expansion as $\mathbf{r}=\mathbf{\Phi a}$. The anisotropy and migration characterization problem is thus reduced to solving the inverse problem $\mathbf{r}=\mathbf{\Phi a}$ for the coefficient vector $\mathbf{a}$.

Since $\mathbf{\Phi}$ is overcomplete, we have an underdetermined set of linear equations and the solution is not unique. However, the dictionary is designed such that a sparse collection of atoms approximates commonly encountered scattering behaviors well. Thus, from the infinite subspace of solutions, we favor those solutions $\mathbf{a}$ that are sparse, i.e. having mostly zero coefficients and a few non-zero coefficients, through a sparsifying regularization approach.

The optimally sparse solution is the solution with the minimum ℓ_0-norm, as the ℓ_0-norm simply counts the number of non-zero entries in a vector; however, finding this sparsest solution is a combinatorial optimization problem in general. The approach we take instead is to minimize a regularization cost function of the form:

$$J\left(\mathbf{a}\right)=\left\|\mathbf{r}-\mathbf{\Phi a}\right\|_2^2+\alpha\left\|\mathbf{a}\right\|_k^k,\ 0<k<1, \quad (7)$$

for which efficient optimization techniques exist [11, 9]. The first term is for data fidelity and the second term is for sparsity, with the tradeoff being controlled by the regularization parameter α; we use $k=0.1$ for the norm in the remainder of this paper.

Let us now consider an example that shows the use of the overcomplete dictionary and sparsifying regularization formulation to characterize both anisotropy and migration within SAR image formation. There is one scattering center in the scene, i.e. $P=1$, with $N=15$ angle samples equally-spaced over a 14° aperture. The scatterer has a certain anisotropy and has circular migration with radius 0.6 meters. The overcomplete dictionary has $L=5$ radii, with the R_l being 0, $\frac{1}{4}$, $\frac{1}{2}$, $\frac{3}{4}$, and 1 meters. These different R_l are illustrated in Fig. 1 along with the true radius of migration overlaid on an image of the scene formed by conventional processing.

The inverse problem is solved with $K=5$ frequencies 9.00 GHz, 9.49 GHz, 9.98 GHz, 1.05 GHz, and 1.10 GHz, by the quasi-Newton optimization method of [11]. As a baseline for comparison, we also solve the inverse problem by least-squares, i.e. the

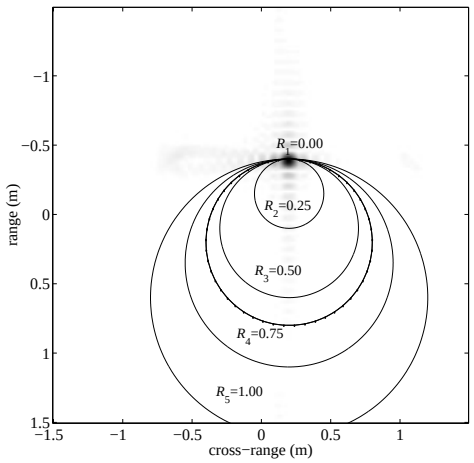

Figure 1: Illustration of atoms of different radii of migration along with true radius of migration, the circle with dots, overlaid on conventionally formed image.

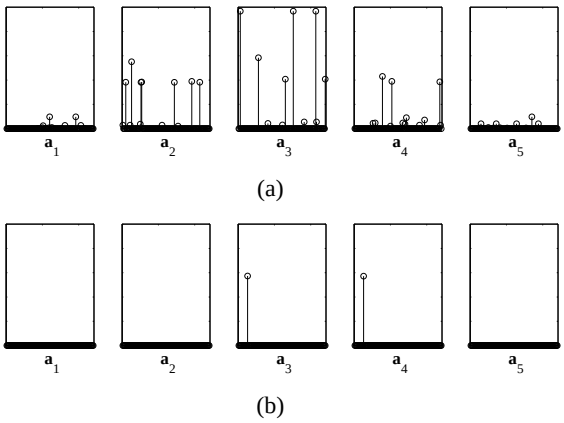

Figure 2: Magnitude of coefficients in (a) least-squares solution and (b) sparsifying regularization solution.

regularization parameter $\alpha = 0$ in (7) and we take the minimum norm solution given by $(\mathbf{\Phi}^H\mathbf{\Phi})^{-1}\mathbf{\Phi}^H\mathbf{r}$. The coefficient magnitudes of the two solutions are shown in Fig. 2 as a stem plot; for ease of interpretation, the coefficients $\mathbf{a}_l$ corresponding to each of the $L = 5$ different radii have been put into separate subplots. Within each subplot, the different coefficients correspond to different types of anisotropy; the coefficients on the left correspond to more isotropic scattering and those to the right, to thin, highly anisotropic scattering. In the least-squares solution many coefficients are non-zero in all of the different radii, whereas in the sparse solution, two of the radii, $R_3 = \frac{1}{2}$ and $R_4 = \frac{3}{4}$, have non-zero coefficients corresponding to the true anisotropy. The true radius, 0.6, falls between $\frac{1}{2}$ and $\frac{3}{4}$, so the solution follows expected behavior.

Through the use of atoms in our overcomplete dictionary that correspond to migratory scattering centers, we are able to parsimoniously represent this phenomenon, and consequently model a region in space rather than a single point or pixel because the area covered by the migration is fully described by the atom. The solution compactly represents the scatterer at the object level. Similarly, we would like to find parsimonious representations for stationary scattering centers that cover extended regions in the spatial domain. An approach proposed in the next section uses properties of the Hough Transform.

4. REGULARIZATION IN HOUGH SPACE FOR GLINT ANISOTROPY

Pixels may be treated as scattering centers, but this ignores the fact that a single point scatterer may correspond to a spatially distributed scattering mechanism. One important type of scattering behavior, glint, which comes from long, flat metal plates is non-migratory, has very thin anisotropy, and corresponds to a line segment in image space oriented at the same angle as the center angle of the anisotropy. A parsimonious representation ought to explain scattering with a single scatterer rather than a collection of scatterers along a line. We extend the regularization cost function (7) to favor sparsity along lines in addition to favoring sparsity among atoms, making use of Hough transform properties and the geometric interpretation they lend.

The Hough transform, which is not a transform in the strict sense, but a method in image analysis for detecting straight lines in binary images [12], uses a ρ-θ normal parameter space that is directly related to the SAR range profile domain, given in expression (2). The normal parameterization uses the angle of a line's normal θ and its algebraic distance ρ from the origin of the image. With x and y as coordinates in the image plane, the equation for a line is $x\cos\theta + y\sin\theta = \rho$.

The parameter space, the ρ-θ plane, and the image space, the x-y plane, are related by the following properties: a point in image space corresponds to a sinusoid in parameter space and a set of points lying on the same line in image space corresponds to a set of sinusoids that intersect at a common point in parameter space. Also, a point in parameter space corresponds to a line in image space and a set of points lying on the same sinusoidal curve in parameter space correspond to a set of lines that intersect at a common point in image space. The Hough transform method of detecting straight lines makes use of these properties.

Let the binary image be such that the background is made up of zero-valued pixels and lines of one-valued pixels. Parameter space is gridded into ρ-θ cells and each one-valued pixel 'votes' for all cells along the sinusoid corresponding to that pixel. If many one-valued pixels are along a common straight line, then their corresponding sinusoids will intersect in one parameter space cell. With parameter space cells acting as accumulators of votes from image domain pixels, a cell with a high count indicates a line in image space. The approach has been extended with different parameters looking for different parameterized curves.

In [13], a Hough space sparsifying regularization approach is employed to enhance and detect straight lines in positive real-valued images by imposing sparsity when taking the image data to the ρ-θ plane. Parameter space cells with small counts are suppressed and cells with large counts are enhanced; thus, non-line features are suppressed and line features are enhanced in image space, making the line detection problem painless. The goals in this paper are different from those in [13] and consequently, the regularization terms are of a different flavor as well: the Hough transform conception of accumulators to detect lines is turned on its head.

The idea is to have sparsity in each cell of the ρ-θ plane rather

than having sparsity among cells. As points on a line in the image domain transform to sinusoids coincident at a point in the range profile domain, sparsity among scatterers in individual ρ-θ cells achieves the goal of sparsity among points on a line. This qualitative description is translated into mathematical terms in the sequel.

The regularization cost $J(\mathbf{a})$ is a function of the coefficient vector $\mathbf{a}$; consequently, in order to work with range profiles, the coefficients must be mapped to that domain first. P separate range profile planes, coming from each of the P scatterers, are required to achieve sparsity among the scatterers in ρ-θ cells.

As mentioned in Sec. 2, the range profile domain and the phase history domain are a single one-dimensional discrete Fourier transform away from each other. Also, the overcomplete dictionary $\mathbf{\Phi}$ is exactly the mapping from coefficients to the phase history domain. However, taking the coefficients through the overcomplete dictionary inherently sums the contributions of each spatial location coherently, which is undesirable when seeking to keep data from the P scatterers separate. Hence, in mapping from coefficients to a set of P range profile planes, a block diagonal matrix $\tilde{\mathbf{\Phi}}$ with $\mathbf{\Phi}_p$, submatrices containing atoms corresponding to spatial location p, on the diagonal is used in conjunction with a matrix $\mathbf{F}$, which is like a DFT matrix. The values are exactly those that would appear in a $K \times K$ DFT matrix, but rearranged to fill an NK by NK area and replicated P times.

Additionally, to select data from a cell $(\rho = \rho_k, \theta = \theta_n)$ in the range profile domain, a matrix $\mathbf{S}_{k,n}$ with P rows and NKP columns composed of mostly zeroes and P ones is used. Specifically, $\mathbf{S}_{k,n}$ is defined as follows with entries indexed by row $i = 1, \ldots, P$, and column $j = 1, \ldots, NKP$:

$$\left(S_{k,n}\right)_{i,j} = \begin{cases} 1, & j = (k-1)N + n + (i-1)NK \\ 0, & \text{otherwise} \end{cases}. \quad (8)$$

Thus, a length P vector of values for an individual range profile cell (ρ_k, θ_n) is obtained by the multiplication $\mathbf{L}_{k,n}\mathbf{a}$, where $\mathbf{L}_{k,n} = \mathbf{S}_{k,n}\mathbf{F}\tilde{\mathbf{\Phi}}$, and has P rows and MP columns. The $\mathbf{L}_{k,n}$ matrices need not be calculated through matrix multiplication; the $\mathbf{F}\tilde{\mathbf{\Phi}}$ product may be calculated analytically in a straightforward manner based on the discrete Fourier transform of the atoms and the operation $\mathbf{S}_{k,n}$ simply involves extracting out the correct elements from the Fourier transform result.

It follows that for sparsity among scatterers in cell (ρ_k, θ_n), a regularization term of the form $\| |\mathbf{L}_{k,n}\mathbf{a}| \|_{0.1}^{0.1}$ is used. Then, continuing to maintain sparsity among atoms, the overall regularization cost function including sparsity in all range profile cells is:

$$J_{\text{line}}(\mathbf{a}) = \|\mathbf{r} - \mathbf{\Phi}\mathbf{a}\|_2^2 + \alpha_0 \|\mathbf{a}\|_{0.1}^{0.1} + \alpha_1 \sum_{k=1}^{K}\sum_{n=1}^{N} \| |\mathbf{L}_{k,n}\mathbf{a}| \|_{0.1}^{0.1}, \quad (9)$$

where we have taken the regularization parameters for all cells to be the same. This extended cost function $J_{\text{line}}(\mathbf{a})$ may be minimized using the quasi-Newton method of [11].

We now present an example that uses XPatch data of glint type anisotropy and shows how the extended cost function with both sparsifying terms, the original one and the new one, leads to a parsimonious representation, whereas a cost with either of the sparsifying terms alone with the data fidelity term does not. The scene contains a single scatterer located at $(0, 0)$ with aspect-dependent scattering as shown in Fig. 3. There are $N = 20$ angles over a 19° aperture centered around zero degrees. There is a spike in scattering response at 5.5°, which is the flash or glint. The figure shows

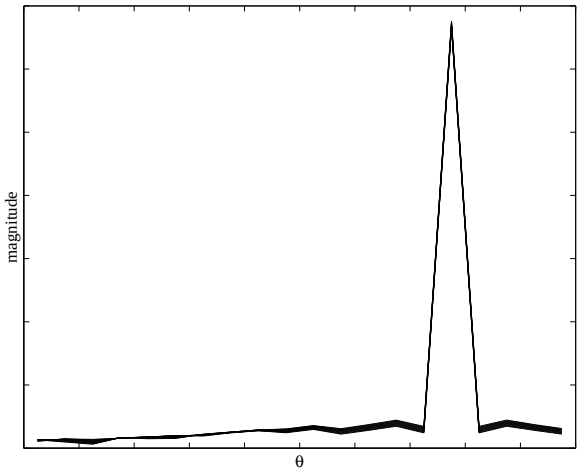

Figure 3: True scattering magnitude of glint anisotropy from XPatch data, with lines for ten different frequency measurements.

the magnitude of the scattering at ten different frequencies in this XPatch data — since there is almost no frequency dependence, the lines are nearly indistinguishable.

In a conventionally formed image using data with a bandwidth of 2 GHz, Fig. 4, the glint shows up as a spread out line segment oriented at 5.5°. From this image, $P = 24$ pixels are chosen as spatial locations for joint anisotropy characterization and image formation. The spatial locations range from $-\frac{9}{90}$ m to $-\frac{1}{90}$ m in the x direction and from $-\frac{1}{90}$ m to $\frac{2}{90}$ m in the y direction, with a uniform pixel spacing of $\frac{1}{90}$ m in both directions.

Then, with $K = 10$ frequencies in the range 9.00 GHz to 9.14 GHz, the anisotropy is characterized with three different pairs of values for the regularization parameters α_0 and α_1. The first set of regularization parameters is $\alpha_0 = 30$ and $\alpha_1 = 0$, i.e. without the extension to the cost function given in (9). The magnitudes of the coefficients for the twenty-four spatial locations are plotted in Fig. 5, arranged as in an image, and the scattering function magnitudes for each of the spatial locations are given in Fig. 6, also arranged as in an image. The anisotropy has been characterized correctly, but split up and assigned to all of the spatial locations. This solution is parsimonious in atoms per spatial location, but is not parsimonious in the number of spatial locations used.

The second set of regularization parameters is $\alpha_0 = 0$ and $\alpha_1 = 20$: just sparsity among spatial locations along a line. As seen in Fig. 7, the solution in this case has non-zero coefficients at just one spatial location. This spatial location is the closest among all $P = 24$ spatial locations to $(0, 0)$, the true location of the scatterer. However, there are many coefficients with large values, not just one as in the previous case. The coefficients and corresponding atoms are such that they add to match the true anisotropy well, as seen in Fig. 8, but the representation is not parsimonious in terms of atoms per spatial location.

The third set of parameters is chosen such that both sparsifying terms in the regularization cost function are significant. With $\alpha_0 = 30$, $\alpha_1 = 20$, the solution coefficient vector has only one non-zero coefficient seen in Fig. 9. The coefficient corresponds to an atom with a single non-zero angle sample, shown in Fig. 10, and is thus parsimonious in both spatial locations and atoms.

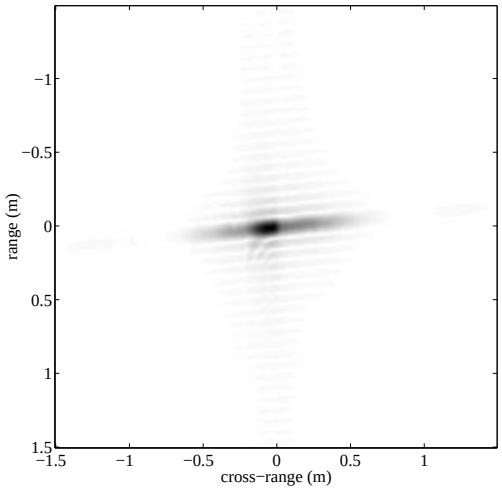

Figure 4: Conventionally formed image of glint anisotropy.

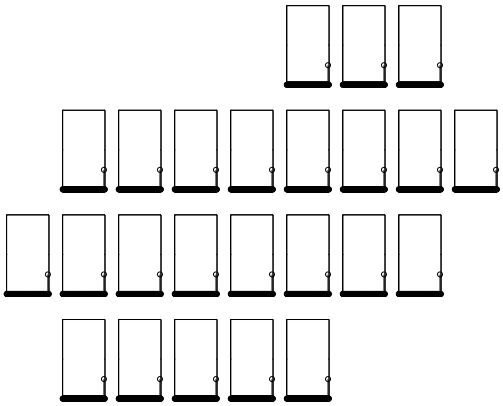

Figure 5: Solution coefficients with $\alpha_0 = 30$, $\alpha_1 = 0$.

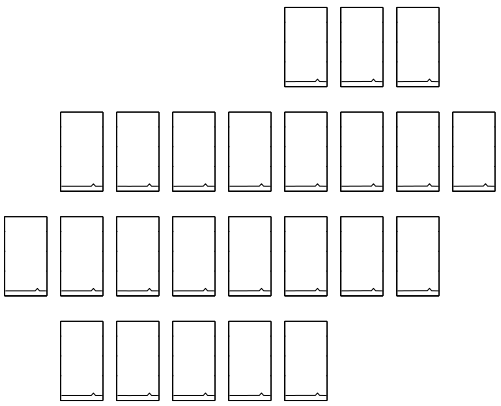

Figure 6: Solution scattering magnitudes with $\alpha_0 = 30$, $\alpha_1 = 0$.

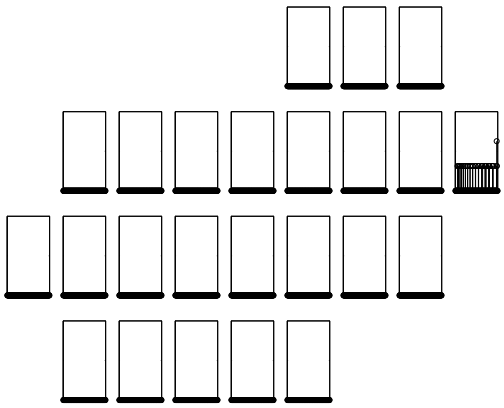

Figure 7: Solution coefficients with $\alpha_0 = 0$, $\alpha_1 = 20$.

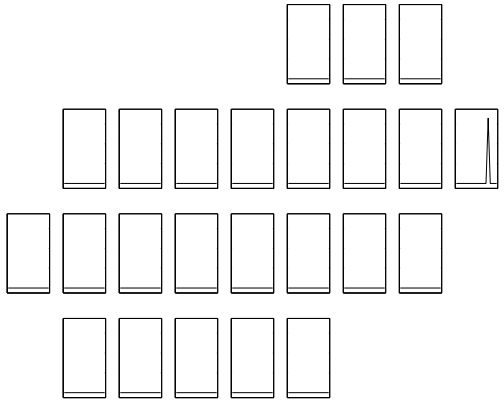

Figure 8: Solution scattering magnitudes with $\alpha_0 = 0$, $\alpha_1 = 20$.

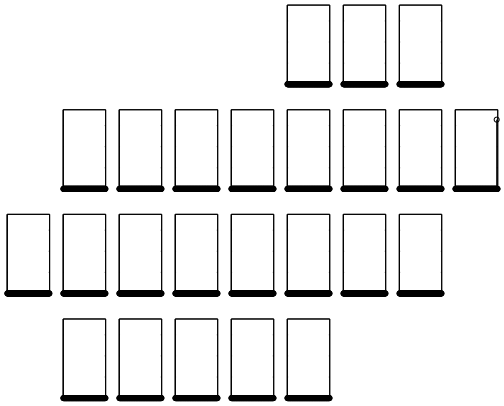

Figure 9: Solution coefficients with $\alpha_0 = 30$, $\alpha_1 = 20$.

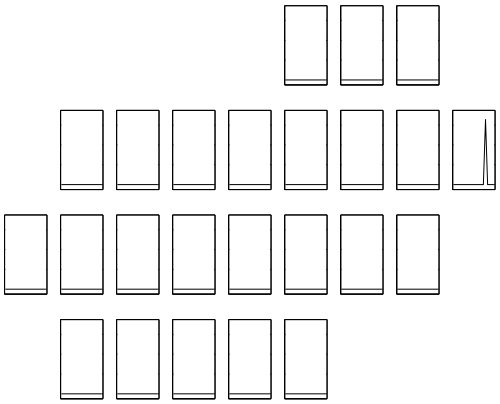

Figure 10: Solution scattering magnitudes with $\alpha_0 = 30$, $\alpha_1 = 20$.

The original sparsifying regularization cost function has the effect of favoring solutions with sparsity among spatial locations because the vector $\mathbf{a}$ has coefficients associated with all spatial locations. The additional regularization terms of this section also favor sparsity among spatial locations because spatial locations along a line are general spatial locations as well. However, the distinguishing characteristic of the additional regularization terms is that the favored sparsity is specially adapted for the object-level idea that individual point-scattering centers affect linear regions in space.

Through the example it has been seen that both types of sparsity — sparsity among atoms and sparsity among spatial locations along a line — are necessary in the regularization in order to recover a solution that represents the scattering as coming from a single point and with very thin anisotropy explained by a single atom. With this representation, spatial properties about the object being imaged, such as orientation and physical extent, may be inferred; thin anisotropy corresponds to objects of large physical extent and wider anisotropy to objects with smaller physical extent. Also, the center angle of anisotropy indicates orientation in the spatial domain. Although the same object-level inferences could have been made with the $\alpha_1 = 0$ solution, in that case, P such objects would be indicated rather than one and having P objects all with large spatial extent almost on top of each other does not make physical sense. Points have more meaning than just pixels with aspect-dependent amplitudes.

5. CONCLUSION

We have extended our overcomplete dictionary formulation for anisotropy characterization in SAR imaging to include atoms representing migratory scattering. By doing so, we move beyond standard pixel-based imaging and are able to describe structures with greater semantic meaning within the image formation process. We are also able to find solutions with higher-level meaning in glint-type stationary scattering through an extension to the sparsifying regularization cost function with additional regularization terms operating in Hough space. These object-level descriptions take us a step farther in the scene understanding chain than conventional image formation while also taking into account phenomena such as anisotropy that cause inaccuracies in conventional methods.

As presented, our approach for the characterization of migration limits solutions to migration along a circle, which often arise with tophats and cylinders. The approach can be further extended to handle non-circular migration through the use of subapertures — finding the best circle over a subaperture and then stitching together circular segments over the full wide-angle aperture. Also, glint and sparsity among points on a line is just one imaging scenario, but an important one; other extensions to the regularization cost function for other scattering phenomena and objects may be developed, either based on properties of the Hough normal parameter space or other parameter spaces and domains.

6. REFERENCES

[1] C. V. J. Jakowatz, Jr., D. E. Wahl, P. H. Eichel, D. C. Ghiglia, and P. A. Thompson, *Spotlight-Mode Synthetic Aperture Radar: A Signal Processing Approach*. Norwell, Massachusetts: Kluwer Academic Publishers, 1996.

[2] R. Bhalla, A. M. Raynal, H. Ling, J. Moore, and V. J. Velten, "Angular description for 3D scattering centers," in *SPIE Defense and Security Symp., Alg. SAR Imagery XIII*, Apr. 2006.

[3] L. C. Potter and R. L. Moses, "Attributed scattering centers for SAR ATR," *IEEE Trans. Image Processing*, vol. 6, no. 1, pp. 79–91, Jan. 1997.

[4] L. C. Trintinalia, R. Bhalla, and H. Ling, "Scattering center parameterization of wide-angle backscattered data using adaptive Gaussian representation," *IEEE Trans. Antennas Propagat.*, vol. 45, no. 11, pp. 1664–1668, Nov. 1997.

[5] A. Genell and D. Lösaus, "On the Cramer Rao bound in determining scattering center parameters using high resolution radar," Master's thesis, Chalmers University of Technology and Göteborg University, Göteborg, Sweden, 2001.

[6] R. D. Chaney, A. S. Willsky, and L. M. Novak, "Coherent aspect-dependent SAR image formation," in *SPIE Symp., Alg. SAR Imagery*, Apr. 1994.

[7] L. R. Flake, S. C. Ahalt, and A. K. Krishnamurthy, "Detecting anisotropic scattering with hidden Markov models," *IEE P. Radar, Son., Nav.*, vol. 144, no. 2, pp. 81–86, Apr. 1997.

[8] M. Çetin and R. L. Moses, "SAR imaging from partial-aperture data with frequency-band omissions," in *SPIE Defense and Security Symp., Alg. SAR Imagery XII*, Mar. 2005.

[9] K. R. Varshney, M. Çetin, J. W. Fisher, III, and A. S. Willsky, "Joint image formation and anisotropy characterization in wide-angle SAR," in *SPIE Defense and Security Symp., Alg. SAR Imagery XIII*, Apr. 2006.

[10] J. B. Keller, "Geometrical theory of diffraction," *J. Opt. Soc. Amer.*, vol. 52, no. 2, pp. 116–130, Feb. 1962.

[11] M. Çetin and W. C. Karl, "Feature-enhanced synthetic aperture radar image formation based on nonquadratic regularization," *IEEE Trans. Image Processing*, vol. 10, no. 4, pp. 623–631, Apr. 2001.

[12] R. O. Duda and P. E. Hart, "Use of the Hough transformation to detect lines and curves in pictures," *Comm. ACM*, vol. 15, no. 1, pp. 11–15, Jan. 1972.

[13] N. Aggarwal and W. C. Karl, "Line detection in images through regularized Hough transform," *IEEE Trans. Image Processing*, vol. 15, no. 3, pp. 582–591, Mar. 2006.